NRC Research Press

ARTICLE

Behaviour of a group of energy piles

Thomas Mimouni and Lyesse Laloui

Abstract: A full-scale experimental site with four energy test piles was built on the campus of the Swiss Federal Institute of Technology in Lausanne, Switzerland. This site was used to investigate interaction effects within a group of energy piles. First, the ground constraints were evaluated by testing the piles without any structure on top. Next, each pile was individually tested once the overlying structure was built, which provided information on the structural constraints and allowed the quantification of the pile–structure–pile interactions. Finally, the four test piles were simultaneously heated to quantify the group effects. A thermal response test was performed on one pile and the thermohydraulic response of the soil between the piles was monitored with piezometers and thermistors. Load redistributions may occur in mixed foundations, i.e., with conventional and energy piles, because of differential displacements. Conversely, heating an entire foundation increases the individual pile displacements, but reduces the differential displacements and consequently the pile thermal efforts. Radial strains may also have a significant impact on the axial thermomechanical response of the piles in stiff soil layers. Heat barely propagated farther than a couple of metres with no significant pore-water pressure variation observed.

Key words: energy pile, full-scale in situ experimental site, group effect, thermomechanical response, thermal response test.

Résumé : Un site d'essais à échelle réelle comportant quatre pieux énergétiques expérimentaux a été construit sur le campus de l'École polytechnique fédérale de Lausanne, en Suisse. Ce site a servi à étudier les effets d'interactions au sein d'un ensemble de pieux énergétiques. Dans un premier temps, on a évalué les contraintes du sol en soumettant les pieux à des essais, en l'absence de structure au-dessus de ces derniers. Puis, une fois cette structure construite, chaque pieu a été mis à l'essai, ce qui a permis d'obtenir des données sur les contraintes structurales en présence et de quantifier les interactions pieu–structure–pieu. Enfin, on a chauffé les quatre pieux expérimentaux afin de quantifier les effets de groupe. Un test de réponse thermique a été effectué sur un pieu et la réponse thermohydraulique du sol situé entre les pieux a été mesurée en continu à l'aide de piézomètres et de thermistances. Des redistributions des charges peuvent avoir lieu dans les fondations mixtes, c.-à-d., dans le cas de pieux conventionnels ou énergétiques, en raison des déplacements différentiels. Inversement, si une fondation est entièrement chauffée, les déplacements de chacun des pieux augmentent alors que les déplacements différentiels, et donc les efforts thermiques à l'intérieur des pieux, diminuent. Les contraintes radiales peuvent aussi beaucoup influer sur la réponse axiale thermomécanique des pieux dans les couches de sol rigides. La chaleur se propage à peine sur quelques mètres au-delà des pieux et aucune variation importante de la pression de l'eau interstitielle n'est observée. [Traduit par la Rédaction]

Mots-clés : pieu énergétique, site expérimental in situ à échelle réelle, effet de groupe, réponse thermomécanique, test de réponse thermique.

Introduction

Energy piles are the most widely used energy geostructures around the world. Bourne-Webb (2013) did a review of existing studies concerning energy piles, which evidenced that there have mainly been thermal performance studies assessing the potential of heat production and storage through these foundation structures. Few studies have explored the mechanical implications of heat exchanges between piles and the ground despite this seeming to be one issue when designing such structures. All the tests carried out to characterize the thermomechanical response of energy piles considered a single pile either under a building, and therefore experiencing real service conditions but somehow extreme, or aside from buildings for testing purposes only. The first test pile was built on the École polytechnique fédérale de Lausanne (EPFL) campus in Lausanne (Switzerland) and was of end-bearing type, resting on a strong sandstone bedrock (Laloui et al. 2003). It was below a real building founded on top of 100 piles, but was the only thermoactive pile, so the constraints acting on it were maximized. This test allowed the thermomechanical response of such a ground heat exchanger to be observed at full scale. An important aspect of this test was that response tests were undertaken at different stages of construction so that the evolution of the pile head constraint was able to be quantified and analysed. This test provided great insight into the thermomechanical response of a single pile below a raft subjected to heating, but was largely overdesigned to prevent possible damage during the tests. Later, Bourne-Webb et al. (2009) tested an isolated pile loaded with a jack mounted on a beam maintained by anchor piles at Lambeth College (London, UK). Thermal loading was achieved using a heat pump and a heat sink pile so that active heating and cooling were possible. A constant load was maintained at the pile head, with no other constraint applied. The test pile was a floating pile, that is to say, embedded within clay without significant pile base resistance. During the test, a period of cooling (–19 °C) was applied to the pile, followed by heating (+10 °C). Murphy and McCartney (2012) investigated the thermal and thermomechanical responses of two energy piles coupled with geothermal boreholes below the Denver Housing Authority Senior Living Facility in Denver, Colorado. The piles were 13–15 m long and 1.1 m in diameter, and they are embedded within a layered soil made of fill

Received 23 September 2014. Accepted 5 May 2015.

T. Mimouni and L. Laloui. Laboratory of Soil Mechanics, Swiss Federal Institute of Technology Lausanne, Lausanne, Switzerland.
Corresponding author: Lyesse Laloui (e-mail: lyesse.laloui@epfl.ch).

Published at www.nrcresearchpress.com/cgj on 6 May 2015.

(~3 m), sand and gravel (~4.6 m), and claystone. Three heat exchange loops were installed per pile, and were subjected to real service conditions. Temperature inside the absorber pipes ranged between 8 and 25 °C depending on the season. It was found that operational conditions would not lead to excessive thermal strains and stresses. Later, Murphy et al. (2014) investigated the response of a piled beam foundation with eight energy piles supporting a small single-storey building. While all eight piles (0.61 m in diameter and 15.2 m long) were thermally activated, only three were instrumented. The local stratigraphy would have allowed a slab-on-grade foundation, but using the piles also provided the heat source. Therefore, the soil can be considered as relatively stiffer than in the previous field tests. An in situ heating test applied a temperature increase up to 21–22 °C, which induced concrete thermal expansion between 20 and 150 με, thermal stresses from 1 to 5 MPa, and pile displacement up to 1.5 mm. However, no interaction effect was investigated.

Therefore, tests carried out during previous field investigations focused on single pile responses. However, mechanical interactions between the piles may occur when only a part of the foundation is thermally activated, which is generally the case (Anstett et al. 2005). As a result, differential displacements between the heat exchanger piles and the conventional piles could develop and induce potential damage to the supported structure. Jeong et al. (2014) numerically investigated the thermomechanical responses of energy pile groups with different layouts, but deplored the lack of experimental data to validate their models.

We therefore propose to present full-scale in situ experiments to quantify the magnitude of interactions that could develop within a thermoactive foundation based on a group of four test piles below a water retention tank.

First, the experimental method is presented along with a description of the experimental site, the type of sensors used and the corresponding data treatments, and the different field campaigns that were conducted. Next, each field campaign is individually analysed and compared to the others to determine the nature of pile–structure–pile interactions. Finally, the analysis of energy pile field data using the axial degree of freedom (*n*-parameter) approach employed in this paper is discussed. In particular, the accuracy of the determination of the mobilizable thermal expansion and the impact of two-dimensional (i.e., radial) effects are analyzed.

Experimental method

Experimental site

A new test site at EPFL was installed 200 m from the first test pile described in Laloui et al. (2003). Similar stratigraphic characteristics were therefore present at each location. Information regarding the depth to and thicknesses of the moraine and sandstone layers was available in the area of the Swiss Tech Convention Center, which allowed the stratigraphy of these deeper layers to be determined. However, no data was available on the same area for superficial alluvium layers, which were therefore extrapolated from Laloui et al. (2003). The stratigraphy summarized in Table 1 was therefore assumed to be present at the site. The rock socket on the new test site was increased from less than 1 m, as shown in Laloui et al. (2003), to almost 9 m to compare the radial thermal expansions of the test piles in soft (depth from 0 to 15.7 m) and stiff (depth from 15.7 to 28 m) soil layers. The impact of blocked or observed radial thermal strains on the axial thermomechanical responses of the piles was then quantified.

The new site includes four energy test piles among the 20 piles supporting a water retention tank collecting rainfall from the Swiss Convention Center roof (Fig. 1*a*). The four test piles are grouped below a corner of the tank to keep them apart from the rest of the foundation, which makes the identification of the pile–structure–pile interactions easier because the conventional piles were not instrumented. The base of the tank raft is a 0.5 m thick reinforced concrete raft, and the tank itself is 2 m high, 25 m long, and 9 m wide. The test piles are 28 m long and 0.9 m diameter bored piles. The reinforcing cages measure 0.76 m in diameter and comprise ten 18 mm diameter longitudinal steel reinforcement bars that are attached to circumferential hoops formed from 9 mm diameter bars spaced every 0.2 m along the cage axis. Vertical loads applied to the piles are 0, 800, 2200, and 2100 kN for piles 1, 2, 3, and 4, respectively. The others piles supporting the raft are shorter and narrower Fundex screw displacement type piles.

Table 1. Stratigraphy of test site.

Height above sea level (m)	Type	Thickness (m)
392.2 (pile top)–390.0	Very soft alluvial clay (A1)	2.2
390.0–384.5	Very soft alluvial clay (A2)	5.5
384.5–376.5	Loose sandy gravelly moraine (B)	8.0
376.5–373.0	Stiff bottom moraine (C)	3.5
373.0–364.2 (pile tip)	Sandstone (D)	8.8

Each test pile was equipped with four 24 m long polyethylene U-loops connected in series. The inlet and outlet of the absorber pipes are thermally insulated and the top of the U-loops are installed 4 m below the pile heads (Fig. 1*b*) to avoid thermal interactions with the tank where hot water is stored during summer and cold water during winter. As a result, the 4 m at the pile tops are not thermally active (Fig. 1*c*). The resulting absorber pipe length per pile therefore reaches 192 m. As the pile diameter did not allow safe bending of the pipes, 180° elbows (used for geothermal boreholes) were used at the tops and bottoms of the U-loops and the absorber pipes were attached inside the reinforcing cages with plastic ties.

Samples of concrete (two per pile on piles 1, 2, and 3) were collected on site to estimate the concrete elastic modulus, E_c, density, ρ_c, and strength, σ_c, using uniaxial compression tests after 28 days of curing. The samples were 32 cm high cylinders with a diameter of 16 cm and results of these tests are compiled in Table 2. Retained values for the concrete elastic moduli of piles 1, 2, and 3 are the average of the measured values on their respective samples. The concrete elastic modulus of pile 4 is an average of the elastic moduli of the three other piles.

The test piles were instrumented to measure their axial thermomechanical response. Single vibrating wire strain gauges (model EM-5 from Roctest) were attached to the reinforcing cages at 2 m centres and oriented parallel to the pile axis. Three axial strain gauges were installed at each pile head to monitor possible pile head rotations and load redistributions (Fig. 2). Pressure cells (model TPC from Roctest) were installed at the base of each pile (attached to a welded cross, see Fig. 2). Pile 1 also had 3 m long optical fibers (SOFO system from Roctest) deployed around the perimeter of the reinforcement cage at the pile head, and at 9 m and 19 m depth to observe radial thermal strains.

Piezometers (PWS model with stainless steel filter from Roctest) and 3 kΩ thermistors (TH-T model from Roctest) were deployed along two boreholes to gain further insight regarding heat propagation and pore-water pressure variations in the soil between the piles (P+T 1 and P+T 2, Fig. 1*a*). Two piezometers were positioned in each borehole, one close to the top of the stiff bottom moraine (approximately 16 m below the tank) and the other halfway to the surface (at 9 m depth in P+T 1 and 5.4 m in P+T 2). The piezometers were already equipped with 3 kΩ thermistors (TH-T model from Roctest) because they used vibrating wire transducers requiring temperature correction. Therefore, temperature profiles were completed with single 3 kΩ thermistors (model TH-T from Roctest) installed at approximately 4 m and 13 m depths in P+T 1 and 1.6, 4.4, and 12 m in P+T 2.

Fig. 1. (*a*) Water retention tank with the test piles, (*b*) absorber pipes, and (*c*) piles with local stratigraphy.

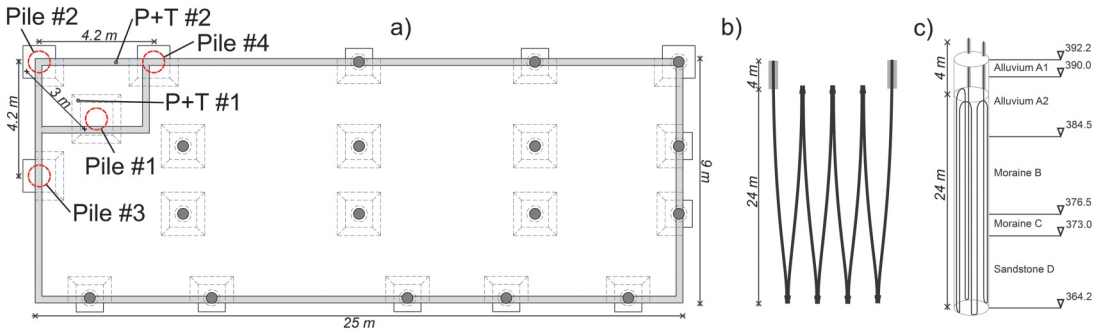

Table 2. Results of uniaxial compression tests on concrete samples after 28 days of curing.

Sample	E (MPa)	σ_c (MPa)	ρ (kg/m^3)
1a	28 000	1.0	2440
1b	27 100	40.5	2460
2a	26 000	44.7	2450
2b	21 100	30.3	2460
3a	23 300	57.9	2450
3b	32 400	55.2	2450

Fig. 2. Pile 1 with pictures of sensors installed on the reinforcing cage.

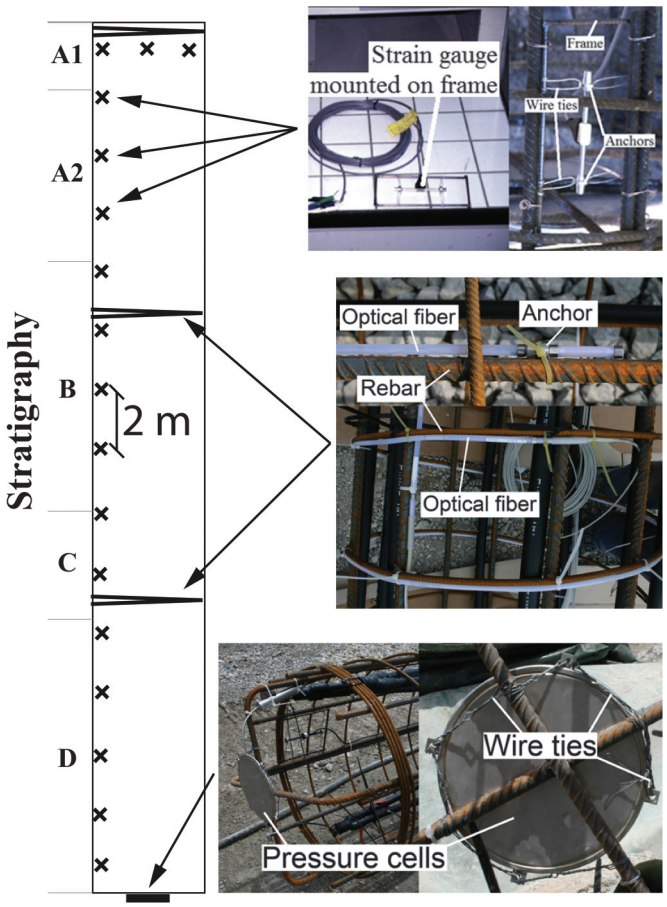

The piles were heated using a thermal response test (TRT) module developed at EPFL (Mattsson et al. 2008). A flow rate of approximately 21 L/min was used during the tests, except on one test during which two piles were connected in series to the same module: head losses caused the flow rate to reduce to 15 L/min. Heat rates were between 2.7 and 3 kW depending on the power supply stability, except during the first test ("free head") during which a lower value (i.e., 1 kW) was tested. Because no active cooling was considered, the heat carrier fluid was water.

Data treatment

The sign convention adopted in this study is as follows: compressive stresses are positive and expansive strains are positive.

Radial optical fibers

Optical fibers require a dedicated reading unit with a pilot computer so that measurements are given as optical fiber lengthening. However, the 3 m long optical fibers, longer than the reinforcing cage perimeter, needed data processing as follows. Let l_{OF} be the optical fiber length (i.e., 3 m), dl_{OF} be the measured optical fiber lengthening, R_{RC} be the reinforcing cage radius (= 0.38 m), and dl_{RC} be the variation in reinforcing cage radius. Assuming that the optical fiber strain is homogenous along its measuring length yields

$$(1) \qquad dl_{RC} = \frac{2\pi R_{RC}}{l_{OF}} dl_{OF}$$

As a result, the variation in reinforcing cage radius becomes

$$(2) \qquad dR_{RC} = \frac{dl_{RC}}{2\pi} = \frac{R_{RC}}{l_{OF}} dl_{OF}$$

Finally, assuming that radial strains are homogeneous in the pile, the variation in pile radius, dR_P, is given by

$$(3) \qquad dR_P = \frac{R_P}{R_{RC}} dR_{RC} = \frac{R_P}{l_{OF}} dl_{OF}$$

where R_P is the pile radius (= 0.45 m). Equation (3) was used to derive the radial strains of the pile from optical fiber measurements.

Vibrating wire strain gauges

Load cells and piezometers equipped with vibrating wire transducers are measured with the same reading unit as the vibrating wire strain gauges, providing the wire resonant frequency and wire temperature. Load cells and piezometers use calibration sheets while the vibrating wire strain gauges require data treatment for temperature correction, based on the vibrating wire theory

$$(4) \qquad \Delta\varepsilon_{ax,obs} = \varepsilon^1_{ax,obs} - \varepsilon^0_{ax,obs} = \frac{K}{1000}(F_1^2 - F_0^2) + \beta^T_{wire}(T_1 - T_0)$$

where $\varepsilon^0_{ax,obs}$ and $\varepsilon^1_{ax,obs}$ are the reference and actual gauge strains, K is a gauge factor provided by the sensor supplier which depends on the wire characteristics, F_0 and F_1 are the reference and actual wire resonant frequencies, β^T_{wire} is the linear thermal expansion coefficient of the wire (= 11.5 με/°C), and T_0 and T_1 are the reference and actual wire temperatures. The resolution of the reading is 0.05 °C for the temperature and 0.05 Hz for the resonant frequency, which yields a global resolution lower than 1 με. Pile maximum head displacements were estimated by integrating the observed thermal strain profiles from pile base to pile head, assuming that the former is fixed (i.e., there is no movement at the pile base).

Strain and temperature measurements allow the estimation of thermal stresses using the axial degree of freedom n, defined as the axially mobilized thermal expansion, $\beta^T_{ax,mob}$, divided by the axial thermal expansion, β^T_{ax}, first assumed equal to the concrete linear thermal expansion, β^T_c (= 10 με/°C, see Choi and Chen (2005); see eq. (5)). Practically, $\beta^T_{ax,mob}$ is determined using linear regression on the $\Delta\varepsilon_{ax,obs}$–$\Delta T$ correlations (Fig. 3). Therefore, this estimation accumulates error when nonlinearity or irreversibility appears in the thermomechanical response of the pile.

$$(5)\qquad \left.\begin{aligned}\beta^T_{ax,mob} &= \frac{\Delta\varepsilon_{ax,obs}}{\Delta T}\\ n &= \frac{\Delta\varepsilon_{ax,obs}}{\Delta\varepsilon_{ax,free}}\end{aligned}\right\} \Rightarrow\quad n = \frac{\beta^T_{ax,mob}}{\beta^T_{ax}} \sim \frac{\beta^T_{ax,mob}}{\beta^T_c}$$

Development of axial thermal stresses results from axial blocked thermal strains due to pile constraints (i.e., ground and supported structure). The latter is estimated from the thermal effect partitioning, which expresses that the free axial thermal strain, $\Delta\varepsilon_{ax,free}$, separates into observed axial thermal strain, $\Delta\varepsilon_{ax,obs}$, and blocked axial strain, $\Delta\varepsilon_{ax,blo}$, as

$$(6)\qquad \Delta\varepsilon_{ax,free} = \Delta\varepsilon_{ax,obs} + \Delta\varepsilon_{ax,blo} = \beta^T_c\Delta T \Rightarrow \Delta\varepsilon_{ax,blo} = \Delta\varepsilon_{ax,free} - \Delta\varepsilon_{ax,obs}$$

The blocked axial strain therefore turns into axial thermal stress, $\sigma_{ax,th}$,

$$(7)\qquad \sigma_{ax,th} = E_c(\Delta\varepsilon_{ax,free} - \Delta\varepsilon_{ax,obs}) = E_c(1 - n)\Delta\varepsilon_{ax,free}$$

from which thermal loads are derived and where E_c is the concrete elastic modulus.

Field campaigns

Three field campaigns were carried out to quantify the interaction effects within the group of test piles. Each thermomechanical test involved heating one (or several) pile(s) with a constant heat rate during approximately 6 days and then letting it return to its undisturbed temperature.

The free head test was completed before the water retention tank construction and only on pile 1 because the construction schedule allowed only a 1 week long test. This test provided information on the ground constraints (i.e., shaft friction and base resistance). The thermomechanical responses of the three other test piles were then assumed to be similar to pile 1 because the piles are identical and close to each other (maximum 4.2 m apart). The heating power was 1 kW during the first 2 days of the test and then 2 kW during last 3 days. This test was of relatively short duration and with low heat rates, which resulted in a low temperature increase in pile 1 of +3.6 °C.

Single pile tests were carried out on each test pile after the tank construction. These tests allowed the quantification of the impact of the tank construction on the individual thermomechanical responses of the test piles. The responses of the unheated test piles were also recorded to quantify the influence of the heated pile on the neighbouring ones: the pile head strains (see Appendix A, Figs. A1–A3) and base compressions were useful to evidence pile head rotations and load redistributions. Pile–structure–pile interactions of first (i.e., directly adjacent piles) and second levels were explored by single pile tests on piles 3 and 4. Heat rates used during single pile tests remained between 2.7 and 3 kW for heating phases of approximately 6 days. Temperature variations in the piles ranged between +6.5 and +10 °C.

Fig. 3. Temperature–strain correlations along pile 3 at 10 m depth (soft alluvium) and 24 m depth (sandstone) during group test.

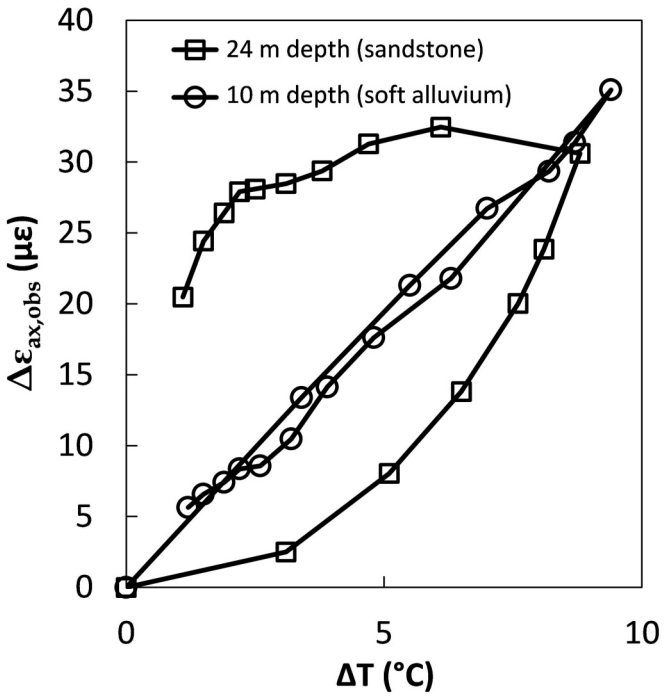

Finally, a group test was undertaken heating the four test piles heated simultaneously. This test provided information on changes in pile constraints due to the global heave of the supported structure when compared to the single pile tests. Piles 1 and 4 were heated individually with heat rates of 3 kW, whereas piles 2 and 3 were connected in series to the same heating module delivering 6 kW, the heat carrier fluid going first through pile 3 and then through pile 2. This 16 day long test comprised 6 days of heating and led to temperature increases in the piles between 7.4 and 9.1 °C.

A 24 day long TRT was also conducted on pile 3. The thermohydraulic response of the soil between the piles was monitored during the free head test, the group test, and the TRT.

Pile axial thermomechanical responses

Free head thermomechanical response test

The evolution of the pile temperature profile during the "free head" test is shown in Fig. 4*a*. Induced thermal load ranged from 90 kN at the pile head to about 560 kN 4 m above the pile base (24 m, Fig. 4*b*). Thermal expansion was observed (Fig. 4*c*), with a maximum of about 30 με recorded in the upper part of the pile, reducing to about 15 με in the lower part.

Little thermal strain was observed along the thermally insulated part of the pile (i.e., the first 4 m) because of climate forcing, because the test was performed during summer with bare soil at the pile top. Thermal strains induced a maximum pile head dis-

Fig. 4. Profiles of (*a*) temperature, (*b*) thermal load, and (*c*) thermal strain – relative displacement during the "free head" test on pile 1.

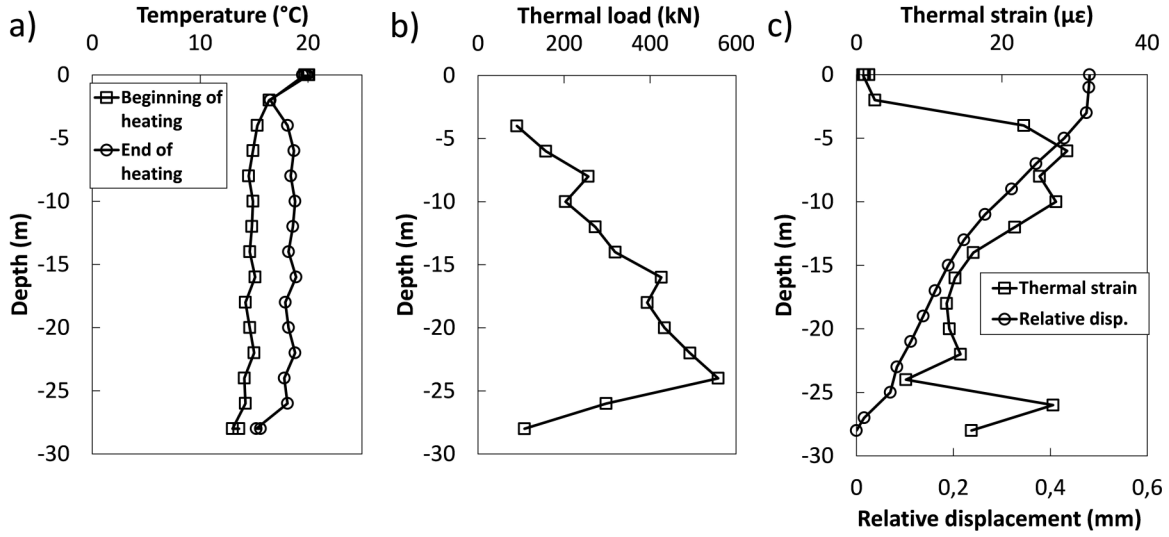

placement of 0.48 mm (Fig. 4*c*). The pile base reaction was monitored, but no significant evolution was observed.

The degree of freedom of the pile under the "free head" configuration decreased from 0.82 at the pile head to 0.14 at a depth of 24 m and increased again up to 0.72 at the pile base (Fig. 5). This profile is characteristic for a pile that has few constraints at its ends, which is the case at the pile head (no structure on top of the pile). However, the particularly high values along the lower part of the pile (i.e., from 22 to 28 m depth) are questionable because the pile is socketed in a very stiff sandstone. This point is discussed later, in the section entitled "Radial strains and axial mobilizable thermal expansion coefficient", where it is shown that the axial degree of freedom is overestimated in stiff soil layers where radial expansion of the pile is prevented.

Fig. 5. Evolution of the degree of freedom profiles from the "free head" test to the single pile tests.

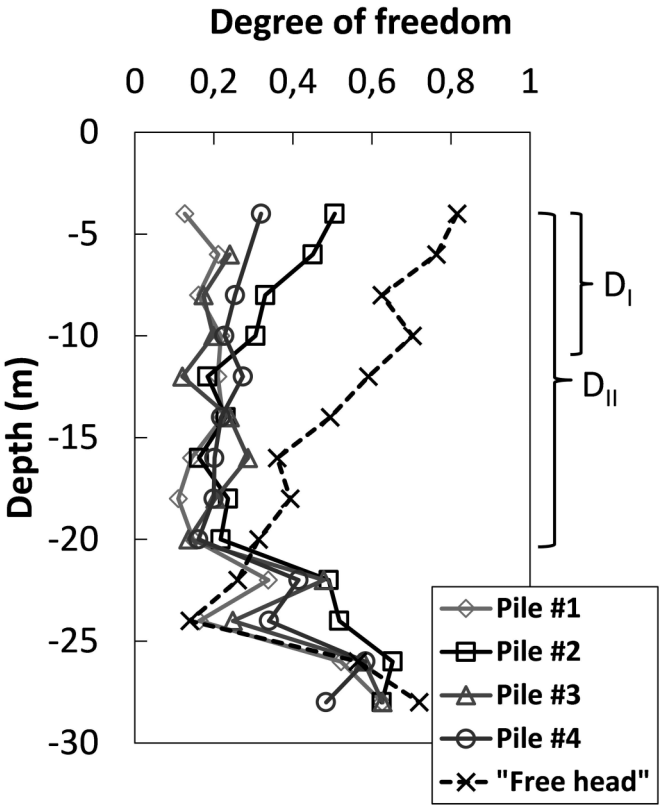

Single thermomechanical response tests

This section presents the results of the single pile tests undertaken after the tank construction. The results are presented in two parts, the first focusing on the individual responses of the heated piles and the second on the pile–structure–pile interactions.

Heated pile responses

The temperature profiles recorded during the single pile tests show relatively constant temperatures along the thermoactive parts of the piles except at the pile bases where boundary effects are significant. Pile temperature increases, averaged along the thermoactive portions of the piles at the end of the heating phases, were 8.5, 9.3, 10.0, and 6.5 °C for piles 1, 2, 3, and 4, respectively (Fig. 6*a*). Profiles of degree of freedom after the tank construction were determined and compared to the "free head" profile (Fig. 5). The degree of freedom of pile 4 might be slightly overestimated as the test on this pile was undertaken only 1 week after the end of the heating test on pile 1; whereas the interval between the other tests was typically 3 weeks. As a result, pile 1 did not fully recover, with a possible slight enhancement of pile 4 thermal expansion. The tank construction affected the pile thermomechanical responses along the first 20 m (see D_{II} in Fig. 5) through the soft soil layers while the pile positions below the tank influence the first 10 m (see D_I in Fig. 5). Indeed, pile 2, which is located below the corner of the tank, is restrained less (higher *n*-values) than pile 1 situated more centrally below the body of the tank. Other studies (Bodas Freitas et al. 2013) also suggest that thermal top boundary conditions could have a significant impact on the axial thermomechanical response of energy piles. However, this phenomena is assumed to remain marginal in the present investigations, because the piles are very close to each other and therefore subjected to very similar thermal boundary conditions.

Therefore, the observed thermal strain profiles are shifted, exhibiting greater thermal strains at the pile bases unaffected by the tank construction (around 50 με) and smaller along the upper parts of the piles, remaining around 15 με for piles 1, 3, and 4 and around 28 με for pile 2 (Fig. 6*c*). Consequently, a larger part of the thermal strains are blocked along the first 20 m of the piles com-

Fig. 6. Profiles of (*a*) temperature at end of heating, (*b*) maximum thermal loads, and (*c*) maximum thermal strains during single pile tests, along heated piles.

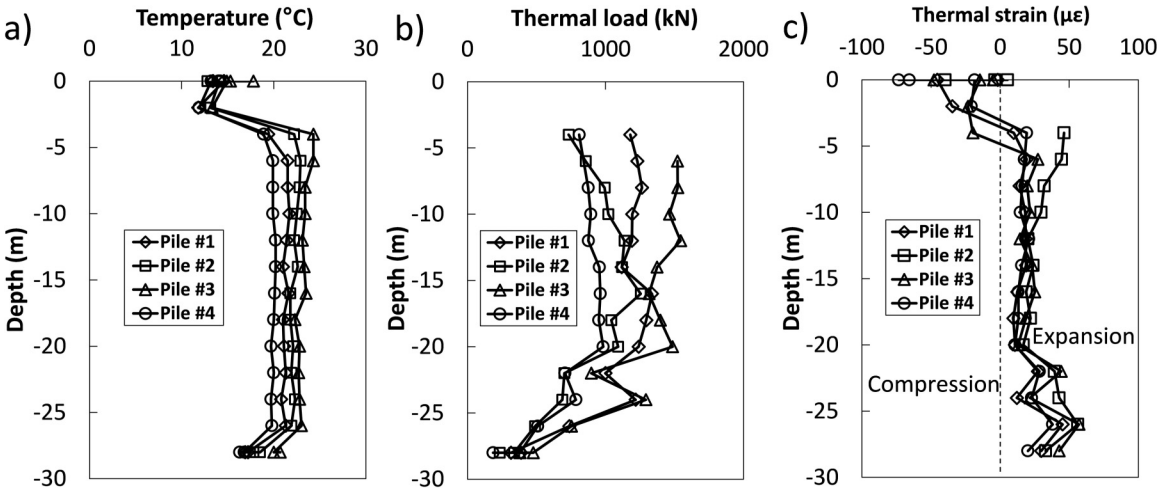

pared to the "free head" configuration, inducing greater maximum internal thermal loads ranging from 983 kN in pile 4 to 1543 kN in pile 3 (Fig. 6*b*). Maximum pile head displacements were 0.36, 0.84, 0.51, and 0.39 mm for piles 1, 2, 3, and 4, respectively.

Pile–structure–pile interactions

Pile–structure–pile interactions were monitored using the three strain gauges deployed at each pile head and the pressure cells at the pile bases. Interestingly, heating a pile resulted in the compression of its thermally insulated top portion because it is trapped between the expanding thermoactive part below and the tank above. In parallel, pile heads of the surrounding test piles experienced expansion. These observations evidence the pile–structure–pile interactions that can develop in foundations including conventional and thermoactive piles. Interactions of first level (i.e., with directly adjacent piles) occur with a factor of 2–5, that is to say, compression observed at the tested pile head is 2–5 times greater than the expansion observed in the directly surrounding piles. Interactions of second level, quantified using tests on piles 3 and 4, showed magnitudes about half those of the first level interactions, as shown in the measurements at the pile heads during the single test on pile 4, Fig. 7. Indeed, the head of the heated pile (pile 4) experienced compression up to 75 με while the closest piles 1 (3 m distant) and 2 (4.2 m distant) expanded up to 20 με. In contrast, an expansion up to 7 με was observed for the second level pile 3 (3 m behind pile 1).

However, the three strain gauges deployed in each pile head did not exhibit the same response. Indeed, for the unheated piles, one shows expansion whereas another experiences compression, unlike the third one, which is almost unaffected. For the heated pile, two strain gauges show similar responses contrary to the third one with no response correlated to the heating and cooling phases, which may result from two phenomena. First, responses not correlated to the test heating and cooling phases (e.g., S1.1, S2.1, or S4.3 in Fig. 7) may be due to the cooling of pile 1 as the test on pile 4 was carried out too soon after to the test on pile 1. Indeed, only 1 week of passive cooling did not allow pile 1 to come back to its initial "isothermal" state. Secondly, the different responses observed within the same pile (i.e., expansion and compression) may be relevant for pile head rotations, the portion of pile facing the heated pile experiencing expansion while the opposite face would experience compression, which is schematically represented in Fig. 8 for the test on pile 4. The rest of the single pile tests are gathered in Appendices A and C.

Pile–structure–pile interactions are visible even down to the pile bases. Indeed, when the base compression increases in the heated pile, it decreases in the surrounding unheated piles. This suggests a load redistribution from the surrounding piles towards the heated pile. Variations in pile base compression observed in the surrounding unheated piles are one order of magnitude lower than the increase observed at the tested pile base because of shaft friction, also involved in the load redistribution process (Mimouni and Laloui 2014). An observation example is depicted in Fig. 9 for the test on pile 1; the others are compiled in Appendix B and gathered in Table 3.

The short delay between the single pile tests of piles 1 and 4 decoupled the responses of these two piles at their bases (see Appendix B, Fig.B1*c*). Indeed, during the heating of pile 4, variations of compression at the base of pile 1 correspond to the cooling of pile 1, still recovering from the previous test, while the variations at the base of pile 4 are well correlated with the heating of pile 4.

First and second level interactions are visible during the test on pile 3, when the base compression observed in piles 1 and 2 reduced by 40 and 15 kPa, respectively, while the base compression on pile 4 shows relief reduction of 5 kPa (see Appendix B, Fig. B1*b*).

Single pile tests allowed the quantification of the impact of the tank construction on the thermomechanical response of the piles and evidenced the pile–structure–pile interactions of first and second orders (see Appendix C, Fig. C1).

Group thermomechanical response test

As a comparison with the single pile tests, the four test piles were heated simultaneously to quantify the group effects. Increases in pile temperatures remain similar to the single pile tests, in the range of 7.4–9.1 °C (Fig. 10*a*). The profiles of degree of freedom of the group test, single pile tests, and "free head" test are compared in Fig. 11. A 0.2 general increase in the degree of freedom is observed along the piles from the single pile tests to the group test, consequently doubling the degree of freedom along the first 20 m of the piles.

As a result, thermal strains observed along the piles increased, around 35–40 με along the first 20 m and around 50 με in the lower part of the pile (Fig. 10*c*). Higher individual pile displacements were observed (from 0.88 to 1.1 mm) in comparison with the single test (from 0.36 to 0.84 mm), whereas differential displacements were found to be significantly reduced because of the generalized group heave (Table 4). Therefore, maximum internal

Fig. 7. Evolution of pile head strains during single test on pile 4. S1.1, S1.2, and S1.3 are three strain gauges deployed at head of pile 1. The same notations are used for three other piles (S2.1, S2.2, S2.3 for pile 2, etc.).

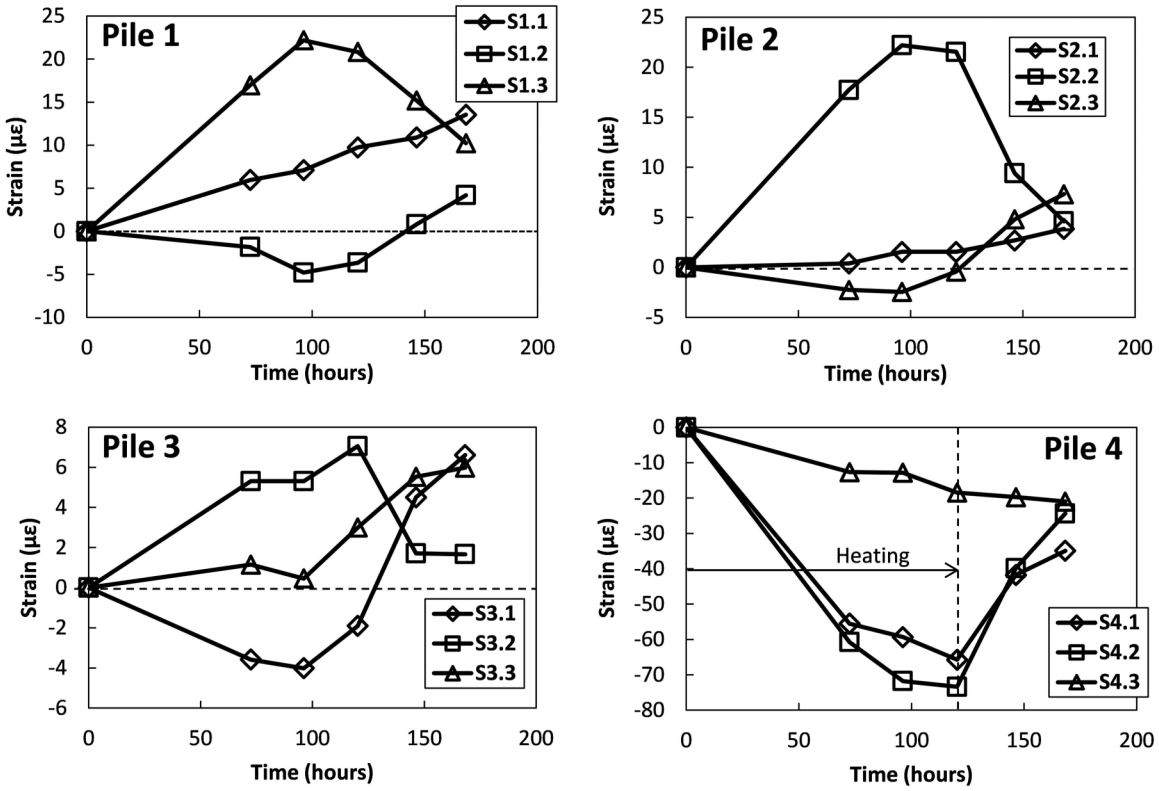

Fig. 8. Schematic representation of pile–structure–pile interactions through raft bending during single test on pile 4. Vertical arrows on top of the piles represent magnitudes of interactions; the cross section displayed beside the piles shows possible induced rotations, the main axis of rotation being represented in grey. The heated pile (pile 4 here) is expanding.

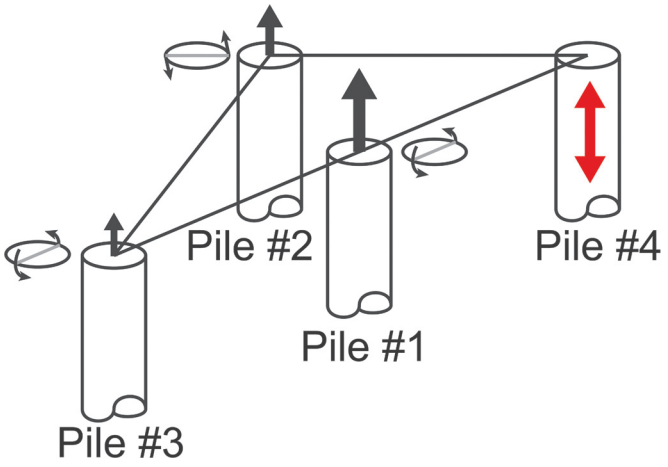

Fig. 9. Pile base compressions during heating of pile 1.

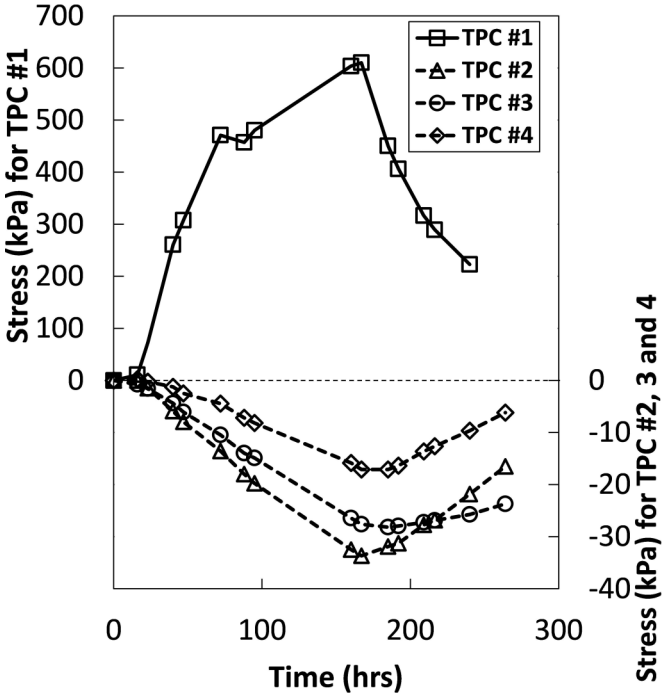

thermal efforts decreased, between 776 and 1100 kN (Fig. 10*b*) with pile base compressions also slightly relieved compared to single pile tests (see Fig. 12 and Table 3).

The constraints applied by the retention tank on the piles were shown to be critical along their first 20 m comparing the "free head" test with the single pile tests. Moreover, single pile tests highlighted the pile–structure–pile interactions between heat exchanger piles and the surrounding conventional piles while the group test evidenced the group effects' significance, inducing a generalized heave, which relatively increased the absolute pile head displacements, but significantly reduced the differential displacements and internal thermal efforts. Results related to the thermomechanical response tests are gathered in Table 4.

Table 3. Variations in pile base compression during single pile tests. Single pile tests correspond to columns, which indicate which pile was heated during each test.

	Pile base compression (MPa)			
TPC	Pile 1	Pile 2	Pile 3	Pile 4
1	610	−47	−40	−53
2	−34	367	−15	−8
3	−28	—	597	−7
4	−17	−16	−5	291

Note: Rows list the different pressure cells (TPC 1 in pile 1, etc.).

Thermal and thermohydraulic responses of the piles and soil

Thermal response test on pile 3

Several attempts to carry out TRTs on energy piles have been reported in the literature. Brettman and Amis (2011) successfully analyzed TRTs performed on 300 and 450 mm diameter and 16.8 m long piles (i.e., aspect ratios of 56 and 37, respectively) using the finite line source theory. Furthermore, Hemmingway and Long (2013) established good agreement between the results from the line source theory with energy piles and the Geothermal Properties Measurement model (described in Hemmingway and Long 2013), therefore increasing confidence in the applicability of the line source theory to energy piles. However, Bouazza et al. (2013) compared results from TRTs carried out on a 600 mm diameter and 16.1 m long piles (i.e., aspect ratio of 27) while using different test durations (9 and 52 days of heating), to TRTs on geothermal boreholes and laboratory tests on samples. The estimated thermal diffusivity based on the energy pile tests were shown to be higher than the others, suggesting that the pile TRTs overestimate the effective soil thermal conductivity. Recently, Loveridge and Powrie (2014*b*) highlighted the weaknesses of the infinite line source model with low aspect ratio piles and proposed a method based on *G*-functions for concrete and ground.

Herein, a 24 day long TRT on pile 3 using a constant heat rate of 3 kW and a flow rate of approximately 21 L/min was analyzed with the infinite line source model given as (Mattsson et al. 2008)

$$(8)\quad \begin{aligned} T_f(t) - T_g &= \frac{q_c}{4\pi\lambda_{eff}}\ln(t) + q_c\left\{R_b + \frac{1}{4\pi\lambda_{eff}}\left[\ln\left(\frac{4\alpha}{r_b^2}\right) - \gamma\right]\right\} \\ T_f(t) &= \frac{T_{in}(t) + T_{out}(t)}{2} \end{aligned}$$

where T_{in} and T_{out} represent the inlet and outlet temperatures of the ground heat exchanger; T_g is the undisturbed ground temperature; $q_c = Q_{th}/H$, with Q_{th} (~3 kW) being the module heat rate, and H (= 24 m) the heat exchanger length, is the linear heat rate; R_b is the heat exchanger thermal resistance (in (K·m)/W); r_b is the heat exchanger radius; α is the soil thermal diffusivity; and γ is the Euler constant (= 0.5772). The analyses comply with the minimum time length $\tau_0 > 5$ (i.e., 12 days assuming a thermal diffusivity of 10^{-6} m^2/s) to get an error less than 10% (Hellström 1991) and with the maximum time length $\tau_0 < 10$ (i.e., 23 days) to minimize end effects (Loveridge et al. 2014), the test pile aspect ratio being 31, where τ_0 is the dimensionless time given as

$$(9)\quad \tau_0 = \frac{\alpha}{r_b^2}t$$

Estimation of the effective thermal conductivity consists of a linear regression along the portion of curve delimited by $\tau_0 = 5$ and 10 (see Fig. 13)

$$(10)\quad T_f(t) - T_g = a_\lambda \ln(t) + b_\lambda \qquad \lambda_{eff} = \frac{q_c}{4\pi a_\lambda}$$

where a_λ and b_λ are the coefficients from the regression. Then, one can estimate the thermal resistance R_b inverting eq. (8) and assuming a soil thermal capacity C_{soil} (here 2.5 MJ/(K·m^3)), the thermal diffusivity α of the soil being estimated using (Mattsson et al. 2008)

$$(11)\quad \alpha = \frac{\lambda_{eff}}{C_{soil}}$$

Capacitive effects were estimated during the test because of the large diameter of the test pile (Pahud 1999). The principle of this method lies in subtracting the heat rate stored in the pile and heat carrier fluid to increase their temperatures from the heat rate injected into the pile. Despite a difference in temperature between the pile and the heat carrier fluid, we assume that the rates at which their temperatures increase remain similar on the time interval $[\tau_0 = 5; \tau_0 = 10]$. Consequently, the heat rate absorbed by the heat exchanger pile, Q_{abs}, is given by

$$(12)\quad Q_{abs} = \frac{\Delta T_{f,\tau_{0,5\to10}}}{\Delta t_{\tau_{0,5\to10}}}C_{TOT} = \frac{T_f(\tau_0 = 10) - T_f(\tau_0 = 5)}{t(\tau_0 = 10) - t(\tau_0 = 5)}C_{TOT}$$

where $\Delta T_{f,\tau_{0,5\to10}}$ is the mean fluid temperature increase from $\tau_0 = 5$ to 10, $\Delta t_{\tau_{0,5\to10}}$ is the time length from $\tau_0 = 5$ to 10 (see Fig. 13), and C_{TOT} is the total heat capacity of the pile given as the sum of the concrete and heat carrier fluid heat capacities, neglecting at first the capacity of the pipe walls

$$(13)\quad C_{TOT} = \frac{\pi D^2 H}{4}\rho_c c_c + \frac{\pi\phi^2 L}{4}\rho_f c_f$$

where D and ϕ are the pile and absorber pipe inner diameters (D = 0.9 m and $\phi = 32 - 2 \times 2.9 = 26.2$ mm), respectively; H is the pile thermoactive part length (24 m); L is absorber pipe total length (192 m); c_c (880 J/(kg·K)) and c_f (4186 J/(kg·K)) are the concrete and heat carrier fluid (water) heat capacities, respectively; and ρ_c (2500 kg/m^3) and ρ_f (1000 kg/m^3) are the concrete and heat carrier fluid densities, respectively.

The injected heat rate therefore becomes

$$(14)\quad q_c = \frac{Q_{th} - Q_{abs}}{H}$$

The soil thermal conductivity estimated considering the capacitive effects is equal to 3.06 W/(m·K), but neglecting capacitive effects yields an approximate thermal conductivity of 3.14 W/(m·K). Thermal resistances with and without consideration of capacitive effects stay similar with values of 0.049 and 0.048 (K·m)/W, respectively. The absorbed heat rate, Q_{abs}, of 76 W was found to be very small, which corresponds to 3 W/m, suggesting that capacitive effects become negligible once the steady state is reached.

Anstett et al. (2005) reported thermal resistances of approximately 0.55 (K·m)/W for 1 m diameter piles with four U-loops and a concrete cover of 10 cm. However, the concrete cover on the test pile measured approximately 7 cm and Anstett et al. (2005) also reported lower thermal resistances for lower concrete covers but different pile diameters. Loveridge and Powrie (2014*a*) reported thermal resistances for a 600 mm diameter pile for different concrete covers and number of pipes, with a thermal resistance of 0.045 (K·m)/W for a concrete thermal conductivity of 1.5 W/(m·K),

Fig. 10. Profiles of (*a*) temperature at end of heating, (*b*) maximum thermal load, and (*c*) maximum thermal strain during group test.

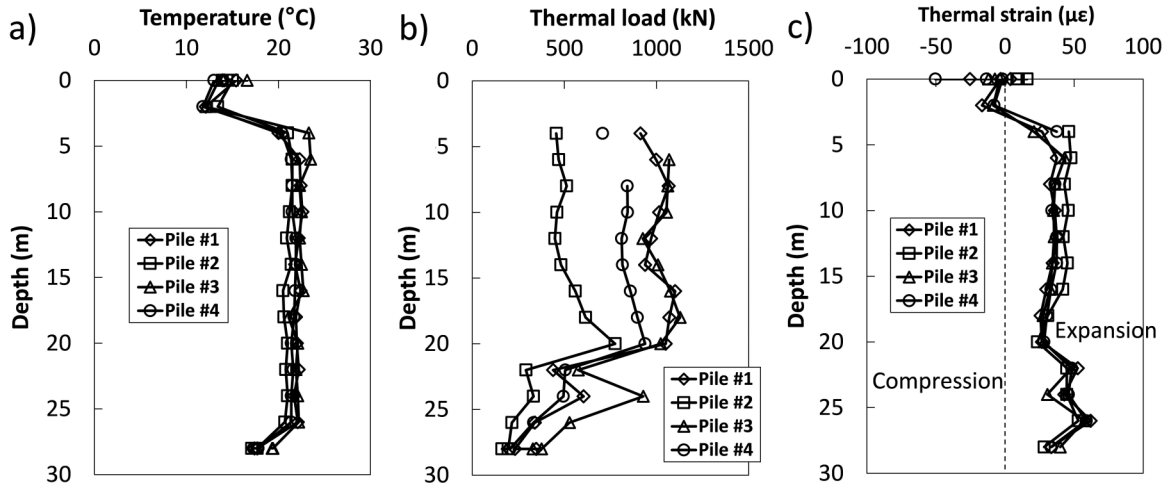

Fig. 11. Evolution of the profiles of degree of freedom from "free head" through single pile tests and to the group test for piles (*a*) 1, (*b*) 2, (*c*) 3, and (*d*) 4.

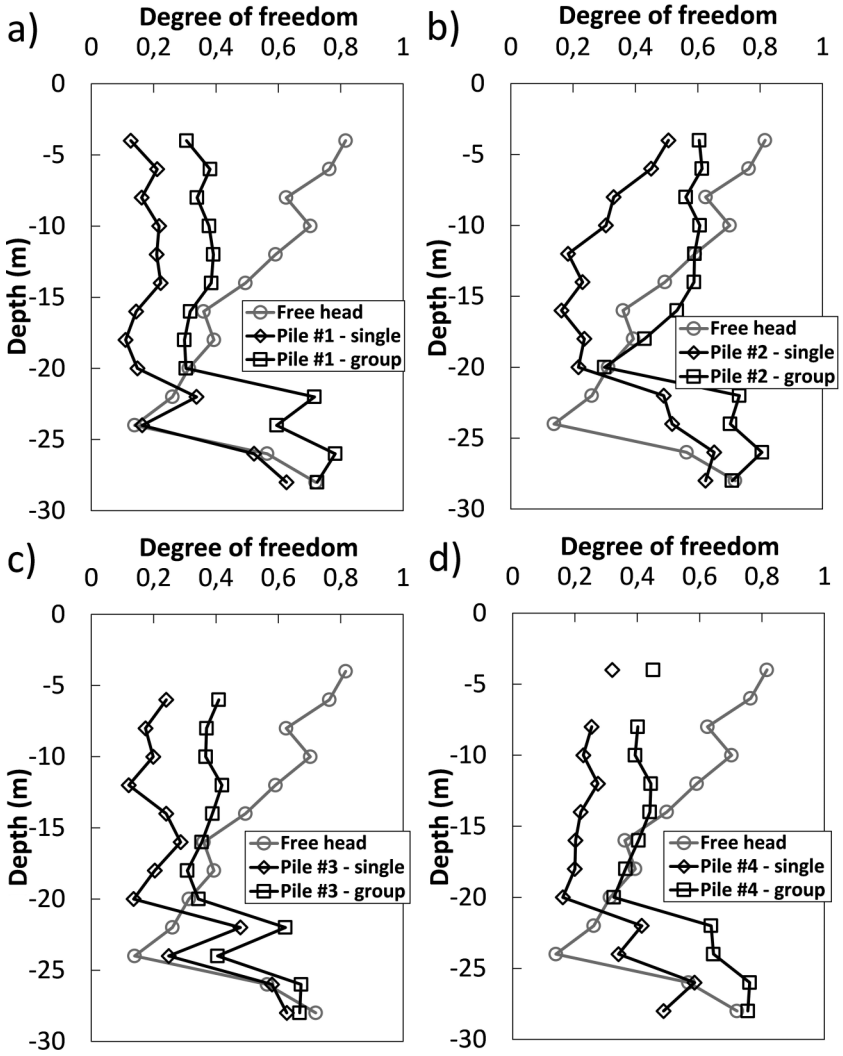

eight symmetrical pipes, and a concrete cover of 7 cm. Poppei et al. (2008) performed a 2 week long TRT on the first EPFL energy test pile which was 25.8 m long and 0.88 m in diameter, but embedded in a similar stratigraphy as in the present test (Laloui et al. 2003). Thus, the pile tested by Poppei et al. (2008) has a similar aspect ratio (~29.4) to those of the piles tested in the present study (~27, taking the thermoactive length equal to 24 m). The main difference lies in the absorber pipe geometry.

Table 4. Main results of thermomechanical response tests.

Test	Pile No.	Heat rate (kW)	Flow rate (L/min)	Max. temp. increase (°C)	Max. pile top disp. (mm)	Max. thermal load (kN)
Free head test	1	1–2	21	3.6	0.48	560
Single tests	1	2.7	21	8.5	0.36	1335.6
	2	3	21	9.3	0.84	1254.6
	3	2.7	21	10	0.51	1543.4
	4	3	21	6.5	0.39	983.1
Group tests	1	3	21	8.5	0.88	1100.9
	2	6	15	7.4	1.1	775.6
	3	6	15	9.1	0.87	1128.0
	4	3	21	8.1	0.96	938.1

Fig. 12. Evolution of pile base compressions during group test.

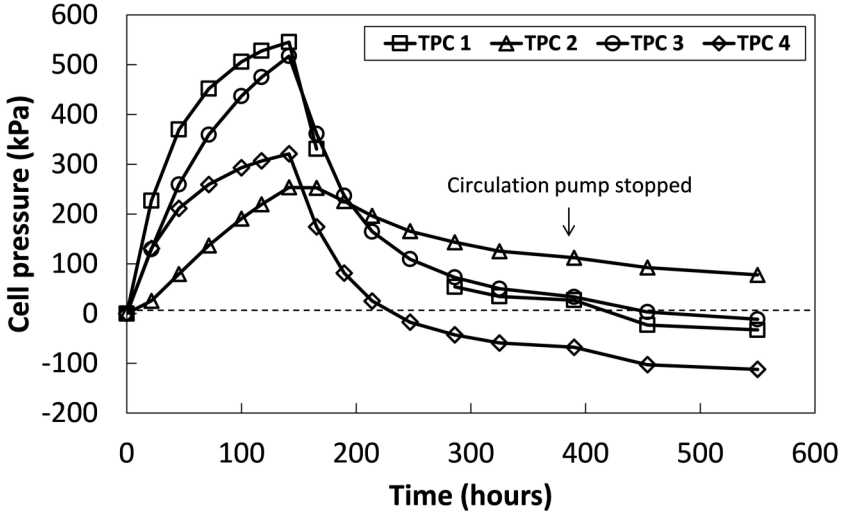

Fig. 13. Analysis of TRT on pile 3.

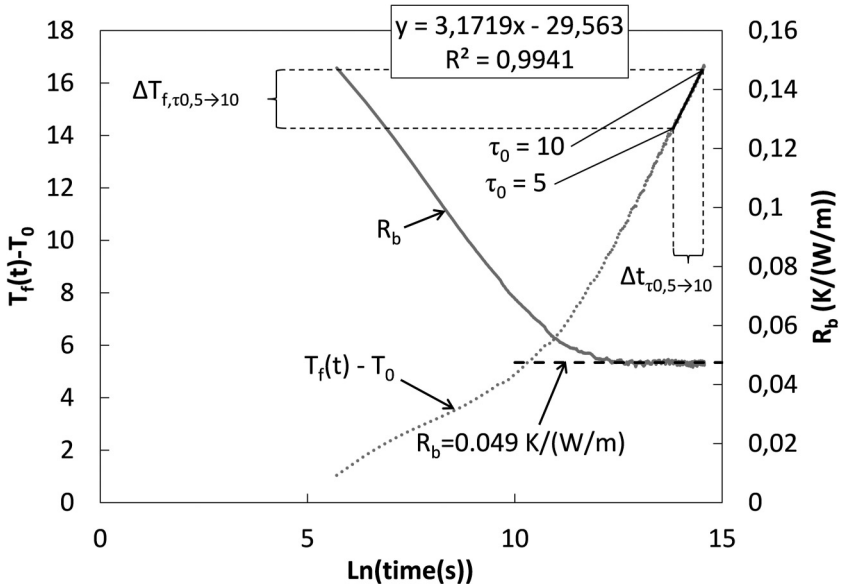

Indeed, the pile test by Poppei et al. (2008) had four U-loops, but they were connected in parallel through connectors at the pile inlet and outlet, while the piles in the present test have four U-loops connected in series. The test conditions were the same as in the present study, that is to say, a flow rate of 21 L/min, and so were the analysis methods. However, Poppei et al. (2008) used a heat rate of 36 W/m, versus 125 W/m in the present test. They estimated a lower pile effective thermal conductivity of 2.74 W/(m·K) and a greater pile thermal resistance of 0.164 (K·m)/W. As a result, it seems that installing the U-loops in series enhances the dissipation of heat towards the ground, which seems consistent with the fact that the heat exchanger length increases by a factor of four when the U-loops are placed in series, compared to the configuration in parallel.

Fig. 14. Profiles of (*a*) pore-water pressure and temperature along (*b*) P+T 1 and (*c*) P+T 2 during the "free head" test.

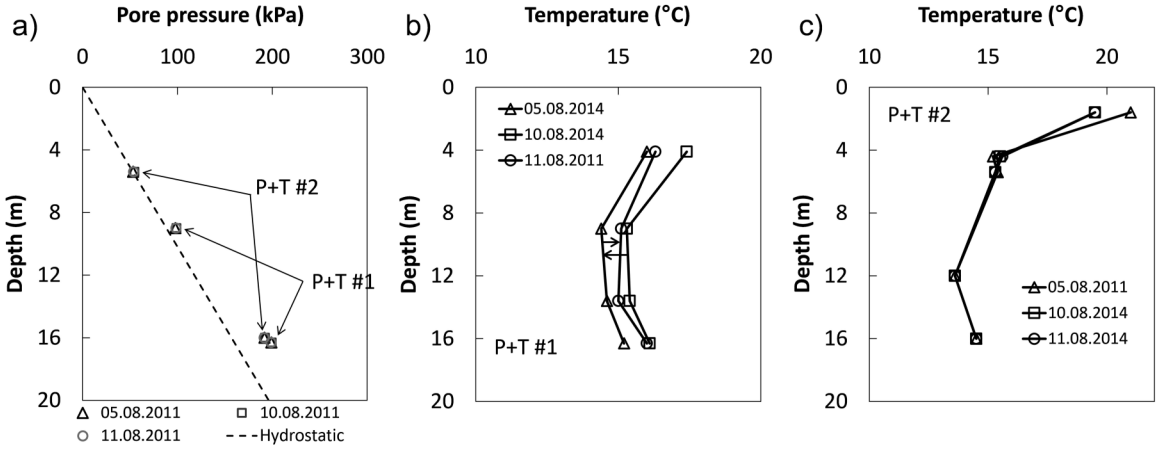

Fig. 15. Evolution of (*a*) pore-water pressure profile, (*b*) pore-water pressure in time, and (*c*) temperature along P+T 1 during group test.

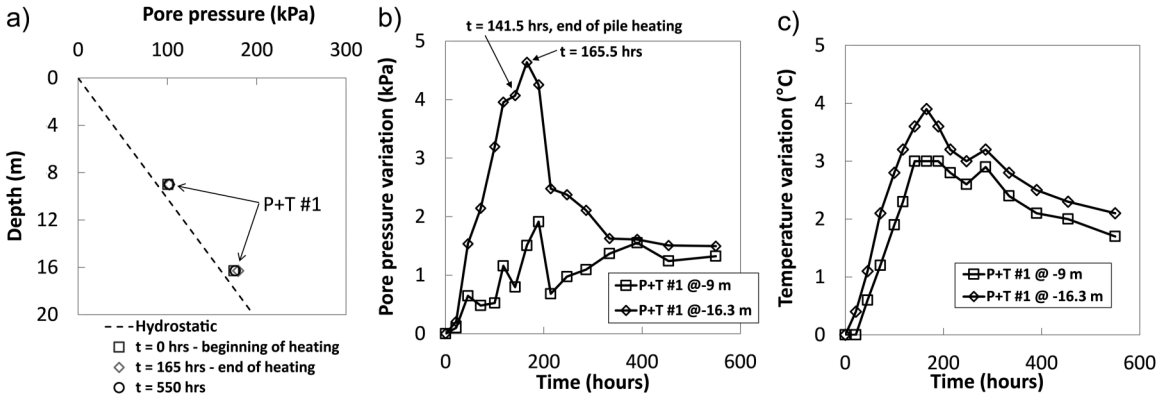

Thermohydraulic response of the soil

The thermohydraulic response of the soil around the test piles was monitored during the "free head" test, the group test and the TRT performed on pile 3. Measurements of the pore-water pressure and temperature profiles along boreholes P+T 1 and P+T 2 were carried out. These boreholes are between piles 1 and 2, and piles 2 and 4, respectively (Fig. 1).

The pore-water pressure profiles observed during the "free head" test exhibit a deviation from the hydrostatic gradient, suggesting a possible impact of the drilling operations on the soft soil layers down to a depth of 16 m. However, no thermal effect on pore water pressure was visible during this test (Fig. 14*a*) despite the temperature having increased by approximately 1.5 °C, along P+T 1, 0.5 m away from the shaft of pile 1 (Fig. 14*b*). The temperature variation did not reach P+T 2 where only surface temperature effects were observed (Fig. 14*c*).

Pore-water pressure observed during the group test shows better agreement with the hydrostatic gradient (Fig. 15*a*). A temperature increase up to 3.5–4 °C observed along P+T 1 (Fig. 15*c*) induced no significant pore-water pressure variation at 9 m depth but an increase of 4.6 kPa at 16.3 m depth (Fig. 15*b*). Comparisons of temperature time series in the pile and along P+T 1 also exhibit a delay of about 24 h. Indeed, the peak in pile temperature occurred 141.5 h after the group test began (i.e., at the end of the heating phase), while the peak along P+T 1 was observed at 165.5 h (Fig. 15*b*). This delay was not further investigated in the present study, but is characteristic of the thermal diffusivity of the ground (Mimouni et al. 2015). Temperature measurements along P+T 2 were not stable during this test and therefore no pore-water pressure estimate could successfully be achieved because of poor temperature correction.

No variation in soil temperature or in pore-water pressure could be observed along P+T 1 during the TRT of pile 3, indicating the temperature variations did not propagate farther than 3 m away from pile 3 although continuous heating with a heat rate of 125 W/m had been used for 24 days.

In this study, heat transport could be observed within the ground over a distance of about 0.5 m. Despite temperature variations up to 4 °C in the ground, pore-water pressure remained not significantly affected and a hydrostatic pore-water pressure profile was observed.

Discussion

Accuracy of the determination of the degree of freedom – mobilizable thermal expansion coefficient

The degree of freedom was estimated following a linear-regression based method. Therefore, the hysteretic behaviours that could be observed, as well as the irreversible strains caused by the elastoplastic response of the soil, may affect the accuracy of these estimates.

The coefficients of determination were computed along each pile to investigate the confidence in the estimated degrees of freedom. Poor coefficients of determination are observed along the pile portions embedded within the sandstone where the pile response is hysteretic (Fig. 3). Thus, estimates with very low coefficient of determination (i.e., lower than 0.7) are not relevant and estimates with relatively low coefficient of determination (i.e., between 0.7 and 0.8) exhibit greater error. However, portions of the piles above the sandstone show good linear trends (see Table 5). The scatter observed at 22 and 24 m depth in the profiles

Table 5. Coefficients of determination, R^2, for the degrees of freedom in the different tests.

		R^2: single pile tests				R^2: group test			
Depth (m)	Free head: Pile 1	Pile 1	Pile 2	Pile 3	Pile 4	Pile 1	Pile 2	Pile 3	Pile 4
4	0.97	0.81	0.99	—	0.99	0.88	1.00	—	0.98
6	1.00	0.96	0.99	0.94	0.98	0.96	0.99	0.99	—
8	0.99	0.99	1.00	0.94	0.96	0.98	0.99	0.99	0.97
10	1.00	0.99	1.00	0.97	0.99	0.99	0.99	1.00	0.99
12	0.98	1.00	0.97	0.91	0.98	0.99	0.99	0.98	0.99
14	0.90	0.98	0.98	0.98	0.97	0.98	0.98	0.99	0.99
16	0.81	0.99	0.96	0.78	0.99	0.98	0.99	0.99	0.98
18	0.91	0.98	0.96	0.94	0.98	0.99	0.95	0.98	0.99
20	0.91	0.90	0.92	0.93	0.98	0.98	0.98	0.87	0.97
22	0.63	0.75	0.83	0.81	0.95	0.39	0.51	0.66	0.71
24	0.73	0.75	0.74	0.57	0.82	0.46	0.52	0.25	0.45
26	0.86	0.91	0.89	0.92	0.97	0.69	0.73	0.84	0.84
28	1.00	1.00	0.87	0.97	0.99	0.99	0.80	0.93	0.84

Note: Shaded cells correspond to low R^2 values for which no good correlations were found.

Fig. 16. Variations in pile radius observed at pile head, 9, and 19 m depth.

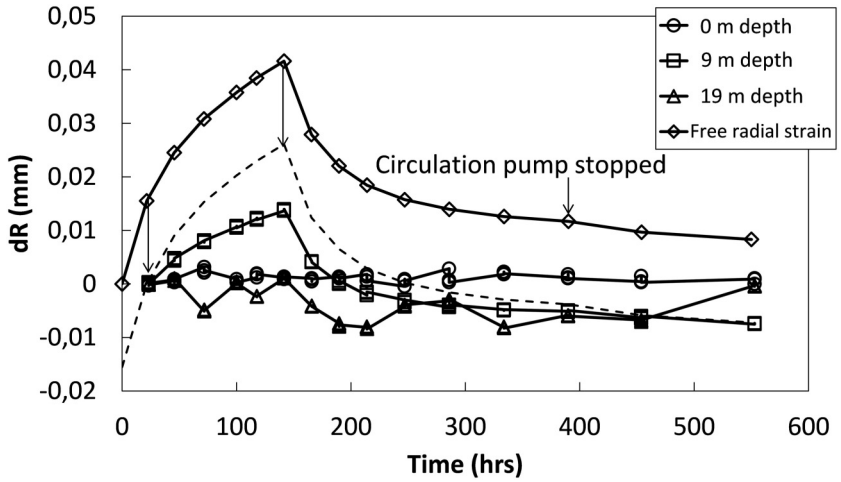

of degree of freedom can therefore be associated with the hysteretic responses in the sandstone.

Radial strains and axial mobilizable thermal expansion coefficient

Radial thermal strains were measured during the group test along pile 1, at the pile head, 9, and 19 m depth. The measurements started 24 h after the beginning of the heating phase because of availability of the reading unit. However, no radial strain was observed at the pile head as this portion is thermally insulated while a clear radial response was shown at 9 m depth, in the soft soil layers. Finally, no radial strain is observed at 19 m depth, suggesting they are blocked in the stiff soil layers. Free radial strains were estimated using the concrete linear thermal expansion of 10^{-5} με/°C and compared to the measured radial strains at 9 m depth.

Despite not having the same initial state, the rate at which the free radial thermal strain increases is much larger than the one measured at 9 m depth, indicating that the radial thermal strains do not occur freely (Fig. 16). The impact of blocked radial strains may have a significant impact on the axial thermomechanical response. Indeed, assuming a thermoelastic response of the concrete pile yields

$$\varepsilon_{ax} = \frac{\sigma_{ax}}{E_c} - \frac{2\nu}{E_c}\sigma_{rad} - \beta_c^T \Delta T$$
$$\varepsilon_{rad} = \frac{\sigma_{rad}}{E_c} - \frac{\nu}{E_c}(\sigma_{rad} + \sigma_{ax}) - \beta_c^T \Delta T \quad (15)$$

Blocking the radial strains ($\varepsilon_{rad} = 0$) and assuming a free axial response ($\sigma_{ax} = 0$) yields

$$\varepsilon_{ax} = -\frac{1+\nu}{1-\nu}\beta_c^T \Delta T \qquad \sigma_{rad} = \frac{E_c}{1-\nu}\beta_c^T \Delta T \quad (16)$$

Therefore, the axial mobilizable thermal expansion coefficient β_{ax}^T becomes

$$\beta_{ax}^T = \frac{1+\nu}{1-\nu}\beta_c^T \quad (17)$$

Consequently, the mobilizable axial thermal expansion coefficient increases by 50% assuming a Poisson's ratio for the concrete of 0.2. Profiles of degree of freedom were therefore corrected using a modified axial thermal expansion equal to 15 με/°C for portions embedded within the stiff soil layers. This correction may partly explain the artificial increase in degree of freedom observed along the lower parts of the piles (Fig. 17).

No correction was applied to the upper part of the thermoactive portions despite partially blocked radial thermal strains, as no direct estimation of the axial mobilizable thermal expansion could be achieved based on the measurements, resulting in a possible slight overestimation of the degree of freedom along the first 20 m of the piles.

Fig. 17. Profiles of degree of freedom with (dashed line) and without (solid line) correction for radial strains: (*a*) free head; (*b*) pile 1; (*c*) pile 2; (*d*) pile 3; (*e*) pile 4.

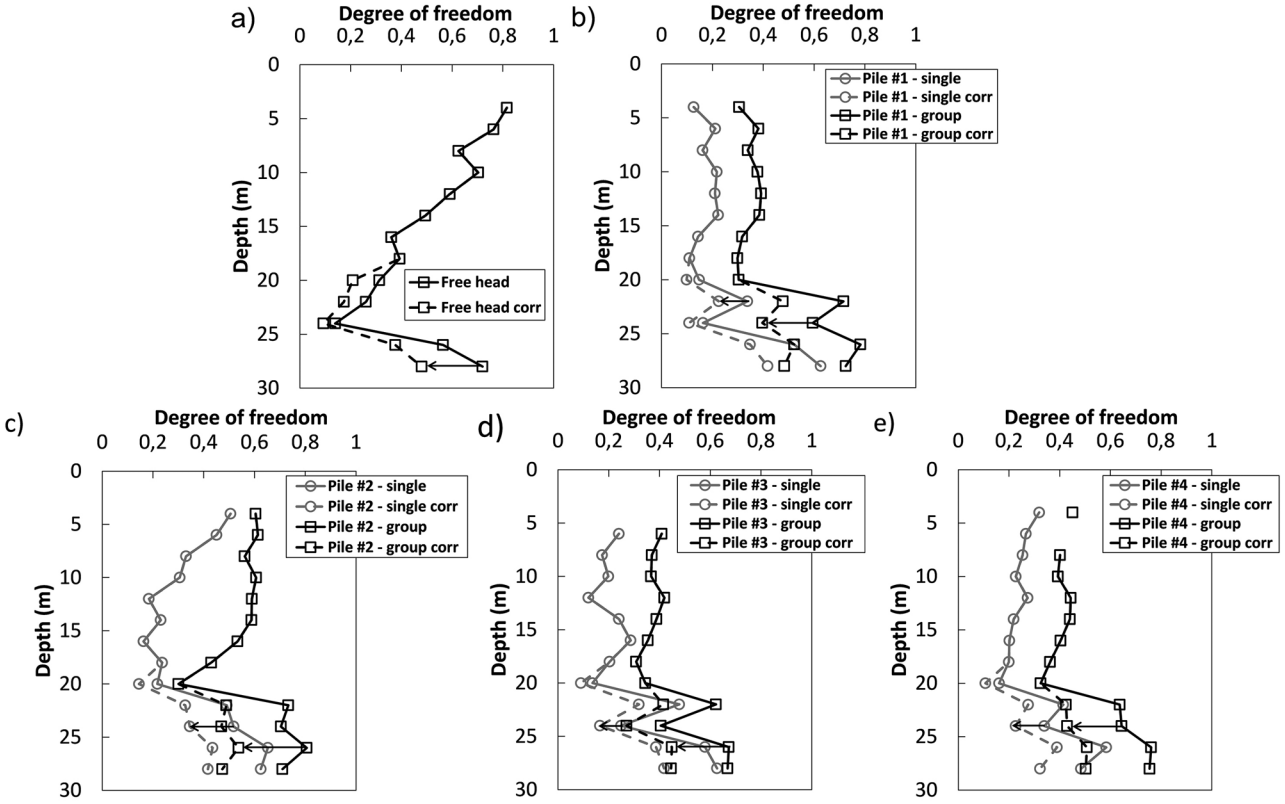

Conclusion

This article presents full-scale in situ experiments, carried out on a group of four energy piles, and their results. The "free head" test, on pile 1, without any structure on top, provided information on the ground constraints acting on the piles. These results were generalized to the three other test piles. Additional single pile tests were undertaken after the water retention tank construction and characterized the individual thermomechanical response of each test pile. It was observed that the tank construction impacted the pile thermomechanical response down to the stiff soil layers while the positions of the piles below the raft influenced the response over the first 10 m of the piles. Furthermore, insulating the first 4 m of the test piles allowed the load redistribution observation within the pile group. Indeed, this allowed removal of thermal effects while analysing load redistributions between the piles. Pile–structure–pile interactions were investigated as the heated pile pulled on the adjacent piles, from pile heads (expansive strains) to pile bases (base compression relieves). During the single pile tests, heated piles exhibited maximum heaves of about 0.84 mm and maximum thermal internal efforts of approximately 1500 kN. The simultaneous heating of the four piles evidenced a significant group effect when comparing the pile thermomechanical responses during the group test and the single pile tests. Indeed, simultaneous heating doubled the piles' degrees of freedom across their first 20 m with increased pile heaves (up to 1 mm) due to greater induced thermal strains, but along with lower differential displacements, resulting in lower internal thermal efforts (up to 1100 kN). We summed the maximum mechanical and thermal stresses experienced during the different tests and found that this number never exceed 15% of the measured average concrete strength (i.e., 45 MN). Therefore, the combination of mechanical and thermal effects are unlikely to cause concrete failure as the concrete strength measured from the samples is between 30 and 58 MPa and the design rules prescribe a concrete strength of at least 25 MPa (i.e., class C 25/30), according to the Swiss Norm SN EN-206-1 (SIA 2013). The main impact of the group effect is then that differential displacements between the test piles are reduced. Indeed, assuming that only the heated pile heaved during single pile tests, differential displacements ranged from 0.36 to 0.84 mm while they remained lower than 0.22 mm during the group test. As a result, the overlying structure is much less solicited on the long term as the magnitudes of cyclic differential displacements are significantly lower.

The development of radial thermal strains was investigated using optical fibers deployed around the perimeter of the reinforcing cage in pile 1 and showed blocked radial thermal strains within the stiff soil and rock layers while they can develop in soft layers. Consequently, the axial mobilizable thermal expansion may increase by 50% within the stiff layers, which should be accounted for in the determination of the degree of freedom profile.

A 24 day long TRT carried out on pile 3 yielded an estimated soil thermal conductivity of 3.1 W/(m·K) and a pile thermal resistance of approximately 0.048 (K·m)/W. Comparing this TRT with the one reported by Poppei et al. (2008) suggests that U-loops in series are more efficient at dissipating heat than U-loops in parallel. The thermohydraulic response of the soil between the piles was monitored using piezometers. Despite temperature variations 0.5 m away from pile 1 reaching 3.5–4 °C during the group test, no variation of pore-water pressure was observed, suggesting a high enough soil permeability to prevent excess pore-water pressure from building up under the thermal load applied during the test.

Acknowledgements

The authors thank L. Gastaldo and J.-F. Mathier from the Laboratory of Rock Mechanics of the Swiss Federal Institute of Technology Lausanne who carried out the compression tests on

concrete samples from the test piles. We also warmly thank F. Dupray and P. Dubey from the Laboratory of Soil Mechanics of the Swiss Federal Institute of Technology Lausanne and G. Steinmann from Swiss Geo Testing Sàrl for their involvements during the test site construction. The financial support of Energie Ouest Suisse Holding, the Swiss Federal Institute of Technology Lausanne, and the Swiss Federal Office for Energy is much appreciated.

References

Anstett, M., Hubbuch, M., Laloui, L., Matthey, B., Morath, M., Pahud, D., Parriaux, A., Rybach, L., Schönbächler, M., et al. 2005. Using the heat from the ground through foundation and retaining concrete structures. Documentation SIA D 0190. Swiss Society of Engineers and Architects. [In French.]

Bodas Freitas, T.M., Cruz Silva, F., and Bourne-Webb, P.J. 2013. The response of energy foundations under thermo-mechanical loading. *In* Proceedings of the 18th International Conference on Soil Mechanics and Geotechnical Engineering, Paris.

Bouazza, A., Wang, B., and Singh, R.M. 2013. Soil effective thermal conductivity from energy pile thermal tests. *In* Coupled phenomena in environmental geotechnics. Torino, Italy. pp. 211–219.

Bourne-Webb, P.J. 2013. Observed response of energy geostructures. *In* Energy geostructures: innovation in underground engineering. *Edited by* L. Laloui and A. Di Donna. ISTE Ltd., and John Wiley and Sons, Hoboken. pp. 45–67.

Bourne-Webb, P.J., Amatya, B., Soga, K., Amis, T., Davidson, C., and Payne, P. 2009. Energy pile test at Lambeth College, London: geotechnical and thermodynamic aspects of pile response to heat cycles. Géotechnique, **59**(3): 237–248. doi:10.1680/geot.2009.59.3.237.

Brettman, T., and Amis, T. 2011. Thermal conductivity evaluation of a pile group using geothermal energy piles. *In* Proceedings of Geo-Frontiers 2011, Dallas, Tex. pp. 499–508.

Choi, J.H., and Chen, R.H.L. 2005. Design of continuously reinforced concrete pavements using glass fiber reinforced polymer rebars. Publication No. FHWA-HRT-05-081. Federal Highway Administration, Washington, D.C.

Hellström, G. 1991. Ground heat storage: thermal analyses of duct storage systems. Ph.D. thesis, University of Lund.

Hemmingway, P., and Long, M. 2013. Energy piles: site investigation and analysis. Proceedings of the ICE - Geotechnical Engineering, **166**: 561–575. doi:10.1680/geng.12.00075.

Jeong, S., Lim, H., Lee, J.K., and Kim, J. 2014. Thermally induced mechanical response of energy piles in axially loaded pile groups. Applied Thermal Engineering, **71**: 608–615. doi:10.1016/j.applthermaleng.2014.07.007.

Laloui, L., Moreni, M., and Vulliet, L. 2003. Comportement d'un pieu bi-fonction, fondation et échangeur de chaleur. Canadian Geotechnical Journal, **40**(2): 388–402. doi:10.1139/t02-117.

Loveridge, F., and Powrie, W. 2014*a*. 2D thermal resistance of pile heat exchangers. Geothermics, **50**: 122–135. doi:10.1016/j.geothermics.2013.09.015.

Loveridge, F., and Powrie, W. 2014*b*. G-functions for multiple interacting pile heat exchangers. Energy, **64**: 747–757. doi:10.1016/j.energy.2013.11.014.

Loveridge, F., Brettman, T., Olgun, C.G., and Powrie, W. 2014. Assessing the applicability of thermal response testing to energy piles. Global Perspectives on the Sustainable Execution of Foundations Works, Stockholm, Sweden.

Mattsson, N., Steinmann, G., and Laloui, L. 2008. Advanced compact device for the in situ determination of geothermal characteristics of soils. Energy and Buildings, **40**(7): 1344–1352. doi:10.1016/j.enbuild.2007.12.003.

Mimouni, T., and Laloui, L. 2014. Towards a secure basis for the design of geothermal piles. Acta Geotechnica, **9**(3): 355–366. doi:10.1007/s11440-013-0245-4.

Mimouni, T., Lei, L., and Laloui, L. 2015. Estimating soil thermal diffusivity with interference analyses. Acta Geotechnica, **10**(2): 197–208. doi:10.1007/s11440-014-0325-0.

Murphy, K.D., and McCartney, J.S. 2012. Behavior of full-scale energy foundations in Denver, Colorado. *In* Proceedings of GeoChallenges: Rising to the Geotechnical Challenges of Colorado. ASCE. pp. 217–229. doi:10.1061/9780784412633.0015.

Murphy, K.D., McCartney, J.S., and Henry, K.S. 2014. Thermo-mechanical characterization of a full-scale energy foundation. *In* From Soil Behaviour Fundamentals to Innovations in Geotechnical Engineering. GSP 233. ASCE. pp. 617–628. doi:10.1061/9780784413265.050.

Pahud, D. 1999. Simulation tool for heating/cooling systems with heat exchanger piles or boreholes heat exchangers. PileSime user's manual. Swiss Federal Office of Energy.

Poppei, J., Péron, H., Silvani, C., Steinmann, G., Laloui, L., Wagner, R., Lochbühler, T., and Rohner, E. 2008. Innovative improvements of thermal response tests. Swiss Federal Office of Energy.

SIA. 2013. Béton - Partie 1: Spécifications, performances, production et conformité. SN EN 206-1/NE:2013. Ed. Société suisse des ingénieurs et des architectes (SIA), Zurich.

List of symbols

a_λ	slope of temperature–ln(time) regression (K or °C)
b_λ	*Y*-intercept of temperature–ln(time) regression (K or °C)
C_{soil}	soil thermal capacity (J/(K·m³))
C_{TOT}	total ground heat exchanger capacity (J/K)
c_c	concrete heat capacity (J/(kg·K))
c_f	heat-carrier fluid heat capacity (J/(kg·K))
D	pile diameter (m)
E_c	concrete Young's modulus (Pa)
F_0	reference resonant frequency (Hz)
F_1	actual resonant frequency (Hz)
H	pile length (m)
K	gauge factor
L	absorber pipe total length (m)
l_{OF}	optical fiber active length (m)
l_{RC}	reinforcing cage perimeter (m)
N	pile axial degree of freedom
Q_{abs}	absorbed heat flux into a ground heat exchanger (W)
Q_{th}	heating power injected into a ground heat exchanger (W)
q_c	linear heat rate along ground heat exchangers (W/m)
R_b	thermal resistance (K·m)/W
R_P	pile radius (m)
R_{RC}	reinforcing cage radius (m)
r_b	ground heat exchanger radius (m)
T_0	reference temperature (K or °C)
T_1	actual temperature (K or °C)
T_f	mean heat-carrier fluid temperature (K or °C)
T_g	undisturbed ground temperature (K or °C)
T_{in}	inlet heat-carrier fluid temperature (K or °C)
T_{out}	outlet heat-carrier fluid temperature (K or °C)
t	time (s)
α	soil thermal diffusivity (m²/s)
β^T_{ax}	maximum mobilizable axial thermal expansion coefficient (K⁻¹)
$\beta^T_{ax,mob}$	axially mobilized thermal expansion coefficient (K⁻¹)
β^T_c	concrete linear thermal expansion (K⁻¹)
β^T_{rad}	maximum mobilizable radial thermal expansion coefficient (K⁻¹)
β^T_{wire}	vibrating wire thermal expansion coefficient (K⁻¹)
γ	Euler constant (= 0.5772)
$\Delta T_{f,\tau_{0,5\to10}}$	temperature variation between τ_0 = 0.5 and τ_0 = 10
$\Delta t_{f,\tau_{0,5\to10}}$	elapsed time between τ_0 = 0.5 and τ_0 = 10
ε_{ax}	axial strain
$\varepsilon_{ax,blo}$	blocked axial thermal strain
$\varepsilon_{ax,free}$	free axial thermal strain
$\varepsilon_{ax,obs}$	observed axial thermal strain
ε_{rad}	radial thermal strain
$\varepsilon_{rad,blo}$	blocked radial thermal strain
$\varepsilon_{rad,free}$	free radial thermal strain
$\varepsilon_{rad,obs}$	observed radial thermal strain
λ_{eff}	soil–pile effective thermal conductivity W/(m·K)
ν	Poisson's ratio
σ_c	concrete density (kg/m³)
σ_f	heat-carrier fluid density (kg/m³)
σ_{ax}	axial stress (Pa)
$\sigma_{ax,th}$	axial thermal stress (Pa)
σ_c	concrete compressive strength after 28 days of curing (Pa)
σ_{rad}	radial stress (Pa)
τ_0	dimensionless time for heat conduction
ϕ	absorber pipe inner diameter (m)

Appendix A. Evolution of pile head strains during single pile tests

Fig. A1. Evolution of pile head strains during single test on pile 1.

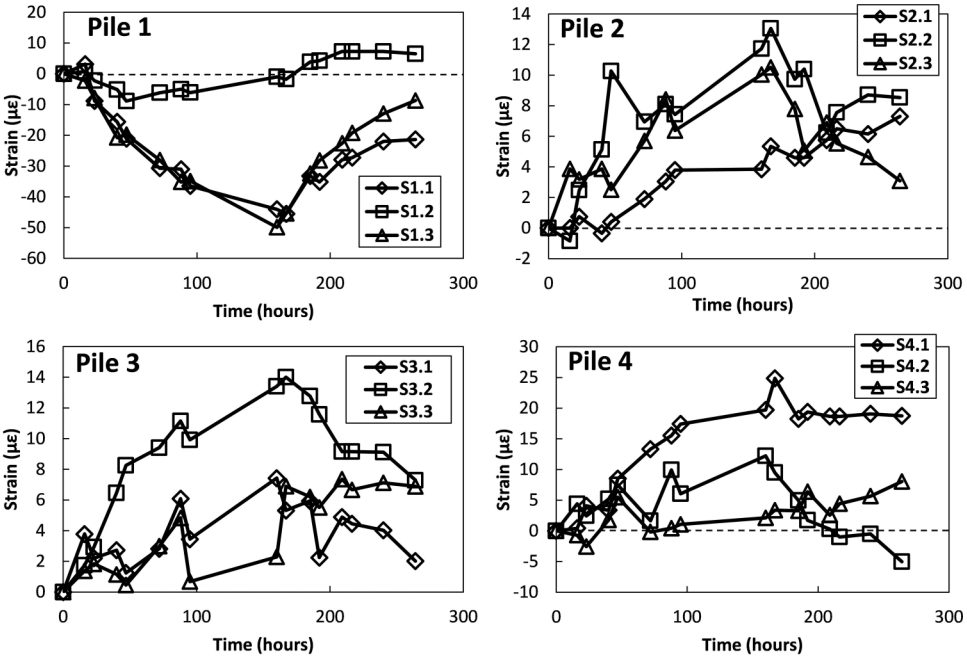

Fig. A2. Evolution of pile head strains during single test on pile 2.

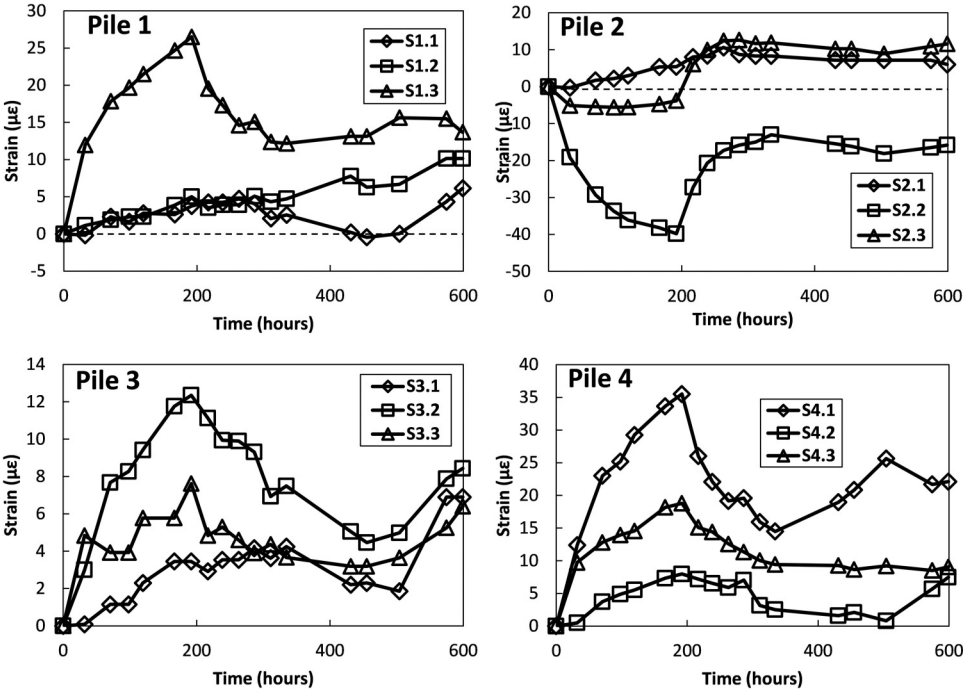

Fig. A3. Evolution of pile head strains during single test on pile 3.

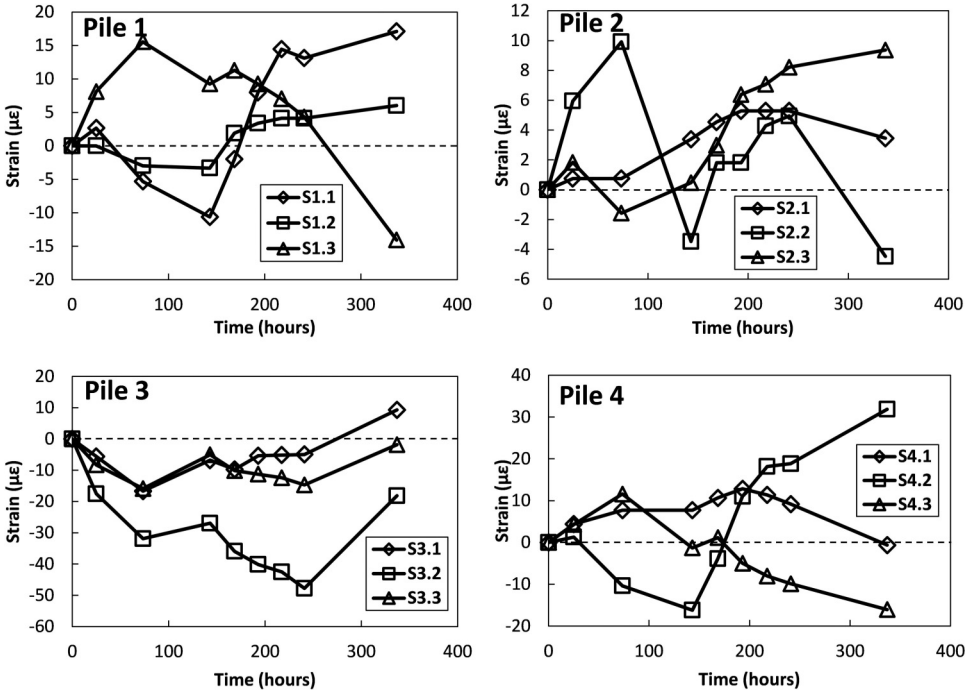

Appendix B. Evolution of pile base compressions during single pile tests

Fig. B1. Evolutions of pile base compressions during single pile tests on piles (*a*) 2, (*b*) 3, and (*c*) 4.

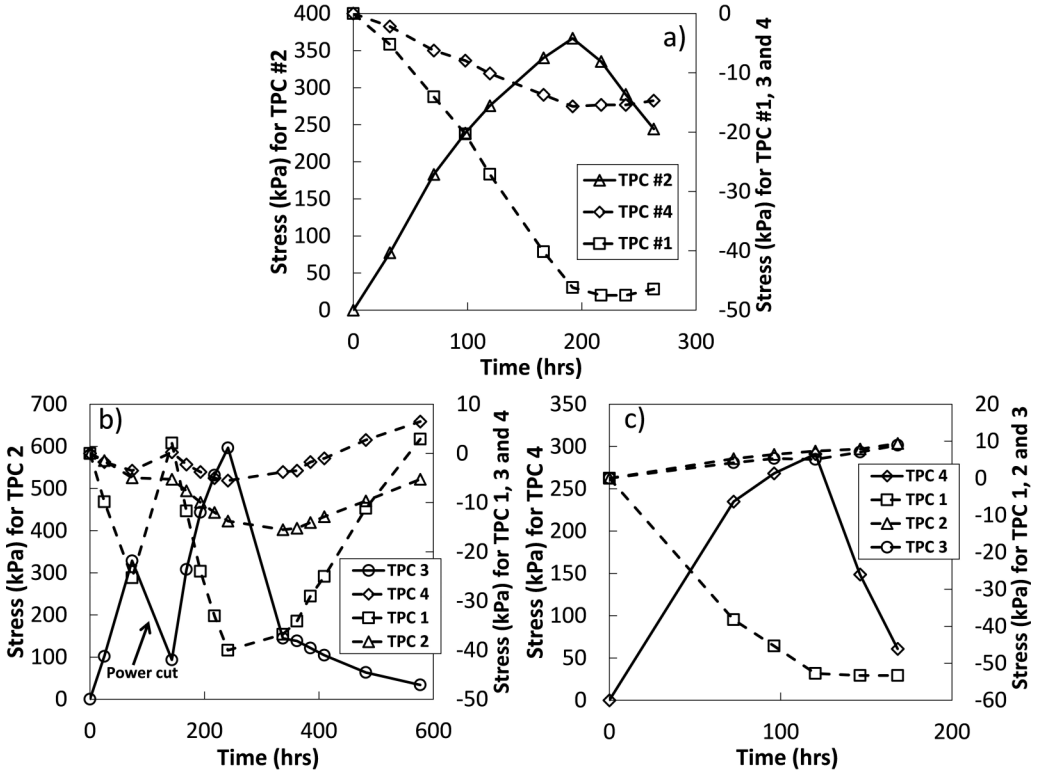

Appendix C. Schematic representation of pile–structure–pile interactions during single pile tests

Fig. C1. Concept of pile-to-pile interactions through raft bending when one pile is heated individually. Vertical arrows on top of the piles represent the magnitudes of the interactions; the cross section displayed beside the piles shows the possible induced rotations, the main axis of rotation being represented in grey. The heated pile is expanding.